

AperTO - Archivio Istituzionale Open Access dell'Università di Torino

Shape controllers enhance the efficiency of graphene-TiO₂ hybrids in pollutant abatement

This is the author's manuscript

Original Citation:

Availability:

This version is available <http://hdl.handle.net/2318/1558125> since 2017-05-24T15:47:41Z

Published version:

DOI:10.1039/c5nr07257c

Terms of use:

Open Access

Anyone can freely access the full text of works made available as "Open Access". Works made available under a Creative Commons license can be used according to the terms and conditions of said license. Use of all other works requires consent of the right holder (author or publisher) if not exempted from copyright protection by the applicable law.

(Article begins on next page)

This is the author's final version of the contribution published as:

Sordello, F; Odorici, E.; Hu, K.; Minero, C.; Cerruti, M.; Calza, P.. Shape controllers enhance the efficiency of graphene-TiO₂ hybrids in pollutant abatement. *NANOSCALE*. 8 (6) pp: 3407-3415.

DOI: 10.1039/c5nr07257c

The publisher's version is available at:

<http://pubs.rsc.org/en/content/articlepdf/2016/NR/C5NR07257C>

When citing, please refer to the published version.

Link to this full text:

<http://hdl.handle.net/2318/1558125>

Shape controllers enhance the efficiency of graphene–TiO₂ hybrids in pollutant abatement

F. Sordello⁽¹⁾, E. Odorici⁽¹⁾, K. Hu⁽²⁾, C. Minero⁽¹⁾, M. Cerruti⁽²⁾, P. Calza^(1*)

¹ Department of Chemistry, University of Turin. Via Giuria, 5, I-10125 Turin, Italy

² Materials Engineering, McGill University, 3610 University St., Montreal, QC H3A 0C5, Canada

Abstract

The addition of graphene nanoplatelets (GNP) to TiO₂ nanoparticles (NPs) has been recently considered as a method to improve the photocatalytic efficiency of TiO₂ by favoring charge carrier separation. Here, we show that it is possible to improve the efficiency of GNP-TiO₂ composites by controlling the shape, stability, and facets of TiO₂ NPs grown on GNP functionalized with either COOH or NH₂ groups, while adding ethylenediamine (EDA) and oleic acid (OA) during a hydrothermal synthesis. We studied the photocatalytic activity of all synthesized materials under UV-A light using phenol as a target molecule. GNP-TiO₂ composites synthesized on COOH-functionalized GNP, exposing {101} facets were more efficient at abating phenol than those synthesized on NH₂-functionalized GNP, exposing {101} and {100} facets. However, neither of these composites was stable under irradiation. The addition of both OA and EDA stabilized the materials under irradiation; however, only the composite prepared on COOH-functionalized GNP in the presence of EDA showed a significant increase in phenol degradation rate, leading to results that were better than those obtained with TiO₂ alone. This result can be attributed to Ti-OH complexation by EDA, which protects GNP from oxidation. The orientation of the most reducing {101} facets toward GNP and the most oxidizing {100} facets toward the solution induces faster phenol degradation owing to a better separation of the charge carriers.

Keywords: TiO₂, functionalized graphene, shape controller

*to whom correspondence should be addressed. Tel: +390116705268, fax: +390116705242. E-mail: paola.calza@unito.it

1. INTRODUCTION

Many pollutants can be abated by photocatalysis, yielding carbon dioxide and dilute acids as final products¹⁻⁶. TiO₂ nanoparticles (NPs) are one of the most widely used photocatalysts⁷, although their efficiency is limited by the fast recombination of the generated electron-hole pairs^{8,9}. Many researchers have tried to improve TiO₂ photocatalytic activity¹⁰⁻¹² with strategies including surface modification with metal particles^{13,14}, semiconductor coupling^{15,16}, or using carbon nanotubes (CNTs) as support^{17,18}. More recently, graphene was suggested as a material able to enhance TiO₂ photocatalytic efficiency by hindering the charge recombination process¹⁹⁻²² thanks to its high charge carrier mobility^{23,24}.

The phase, size, shape and extent to which different TiO₂ facets are developed govern TiO₂ activity^{25,26}. While the {101} facets are the most thermodynamically stable in TiO₂ anatase, the {001} facets exhibit higher reactivity²⁷ and enhanced oxidising ability²⁸ (Scheme 1). Indeed, Ohno and coworkers²⁹ demonstrated that photogenerated holes and electrons can be trapped onto different TiO₂ surfaces, namely electrons on {101} and holes on {001} facets, leading to charge carrier separation.

On properly designed TiO₂ NPs, with both kinds of facets sufficiently developed, charge carrier recombination could be further suppressed thanks to coupling to graphene, which can scavenge electrons from TiO₂³⁰. This synergistic effect can arise provided that the most reducing {101} facets are exposed towards graphene, while the most oxidising {001} facets are in contact with the solution, thus maximising the degradation of dissolved organic compounds.

In a previous work, we used functionalized graphene nanoplatelets (GNP) as a substrate to control phase, shape and exposed facets of TiO₂ NPs in GNP-TiO₂ nanocomposites³¹. We showed that both amino and carboxylate functions on GNP (designed as NH₂-GNP and COOH-GNP, respectively) were able to change the morphology of TiO₂ NPs grown during hydrothermal synthesis, and we reported for the first time TiO₂ NPs resting on graphene sheets with the most reducing {101} facets.

In the present work, we measure the photocatalytic activity towards the degradation of phenol of NH₂-GNP-TiO₂ and COOH-GNP-TiO₂ and we extend the range of GNP-TiO₂ composites by adding shape controllers during the hydrothermal synthesis to improve their catalytic activity and stability under irradiation. We selected either ethylenediamine (EDA) or oleic acid (OA), because they are known to favor the growth of different crystalline facets, namely {100} and {101} for EDA and {001} for OA, leading to elongated or pseudo-cubic

anatase particles, respectively³². Owing to EDA or OA complexation, these facets will not be in close proximity of GNP, but they will likely be oriented towards the solution, thus affecting the charge carrier separation process and therefore the photoactivity and the stability of the hybrid materials.

In principle, shape controllers may compete with GNP surface functions (COOH or NH₂) for TiO₂ surface sites; however, we observed³¹ that the complexing ability of GNP surface groups is limited, and their effect on TiO₂ NP shape is due to local pH changes during NP growth. Still, the addition of shape controllers, in the absence of GNP complexation, may deeply affect the interaction between functionalized GNP and TiO₂. Indeed, our results demonstrate that the addition of EDA or OA leads to the formation of composites with different degrees of association between GNP and TiO₂ NPs. We find that loose coupling can be beneficial for both material stability and photocatalytic activity, and that composites formed on COOH-GNP in the presence of ethylenediamine (EDA) as shape controller provide larger and stable photocatalytic activity than TiO₂ alone.

2. EXPERIMENTAL

2.1. Materials

Graphene nanoplatelets (GNP) were purchased from Graphene Supermarket (3 nm flakes, grade AO1). 4-aminophenyl acetic acid (ACS reagent 99%), sodium nitrite, hydrochloric acid 0,5 M, thionyl chloride (SOCl₂), ethylenediamine (EDA, ACS reagent 99%), isopropyl alcohol, titanium (IV) isopropoxide (TIP, ACS reagent 97%), triethanolamine (TEOA, ACS reagent 99%), oleic acid (OA, ACS reagent 99%) and phenol were all purchased from Aldrich and used as received without further purification. Acetonitrile (AC0331 Supergradient HPLC grade eluent) was purchased from Scharlau. All aqueous solutions were prepared with ultrapure water Millipore Milli-QTM.

2.2 Synthesis of TiO₂-GNP composites

GNP with either carboxylic (COOH-GNP) or amino (NH₂-GNP) groups were prepared and coupled to TiO₂ by synthesizing TiO₂ NPs in-situ, directly on the functionalized GNP either with or without the addition of oleic acid (OA) or ethylenediamine (EDA) as shape controllers.

2.2.1 Graphene surface modification

2.2.1.1 Carboxylic groups. COOH-GNP samples were prepared using diazonium chemistry, as described in ³¹ and Scheme S2. Details on the synthetic procedure is reported as SI.

2.2.1.2 Amino groups. We synthesized NH₂-GNP samples via chlorination and amidation of COOH-GNP as described in ³¹ (Scheme 2). Details on the synthetic procedure is reported as SI.

2.2.2 Graphene-TiO₂ coupling

We prepared GNP-TiO₂ samples by synthesizing TiO₂ NPs directly on GNP with a hydrothermal method³¹. Similarly to³¹, we used the Ti-TEOA 1:2 complex as precursor for TiO₂, prepared pouring 50.0 mmol of titanium (IV) isopropoxide (TIP) in 100 mmol of triethanolamine (TEOA) and bringing to 100.0 ml with deionized water. We put 6.00 ml of TIP-TEOA precursor in a Teflon-lined autoclave together with 7.5 mg of functionalized GNP and, in some of the samples, also 0.06 mmol of shape controller, either OA or EDA. We brought the volume of the mixture to 60 ml and we adjusted the pH to a value among 9.5 and 10. The hydrothermal treatment took place at 110°C for 24 h and then 145°C for 72 h.

To compare the photocatalytic activity of the hybrid materials with that of TiO₂ alone, we prepared TiO₂ NPs in the same conditions, with or without addition of EDA, and carried out their hydrothermal synthesis in the absence of GNP.

Table 1 summarizes all the samples studied in this work.

Table 1: Samples studied in the present work.

Name	Functional Group on GNP	TiO₂	Shape Controller
GNP	None	None	None
NH₂-GNP	NH ₂	None	None
COOH-GNP	COOH	None	None
TiO₂	NO GNP	yes	None
TiO₂-EDA	NO GNP	yes	EDA
NH₂-GNP-TiO₂	NH ₂	yes	None
NH₂-GNP-TiO₂-EDA	NH ₂	yes	EDA
NH₂-GNP-TiO₂-OA	NH ₂	yes	OA

COOH-GNP-TiO₂	COOH	yes	None
COOH-GNP-TiO₂-EDA	COOH	yes	EDA
COOH-GNP-TiO₂-OA	COOH	yes	OA

2.3. Photocatalytic tests

We chose phenol as a target molecule to investigate the photocatalytic efficiency of the materials synthesized in this work. We placed 5 ml of an aqueous solution containing phenol (10 mg l⁻¹) and the catalyst at the desired concentration Pyrex glass cells, and irradiated the solution under stirring, using a TL K05 UV/A lamp, with power of 25 mW m⁻² and emission maximum at 365 nm. We ran all the experiments without controlling the solution pH. After illumination, the entire content of each cell was filtered through a 0.45 µm filter and then analyzed.

We followed the disappearance of phenol as a function of irradiation time using high pressure liquid chromatography (HPLC, Merck-Hitachi L-6200 pumps), equipped with a Rheodyne injector, an RP C18 column (Lichrochart, Merck, 12.5 cm x 0.4 cm, 5 µm packing) and a UV-Vis detector (Merck Hitachi L-4200) set at 220 nm. We eluted the samples with acetonitrile and phosphate buffer (0.01 M) at pH 2.8 (40:60 % v/v) at a flow rate of 1 ml min⁻¹.

3. RESULTS AND DISCUSSION

3.1. Photo-induced phenol degradation with functionalized GNP/TiO₂ hybrids

By functionalizing GNP with either carboxylic (COOH) or primary amino (NH₂) groups we were able to control phase, shape and exposed facets of TiO₂ nanoparticles in GNP-TiO₂ nanocomposites, as shown in ³¹. NH₂ groups favored the growth of TiO₂ bipyramids with higher truncation ratio than those synthesized on GNP modified with COOH groups (Figure S1). Also, NH₂ functionalization favored the coupling between GNP and {001} or {100} anatase facets, whereas COOH groups favored the coupling between GNP and {101} faces. This implies that the TiO₂ NPs found in COOH-GNP-TiO₂ exposed mostly the {001} faces towards the environment. Owing to the different properties of anatase {001} and {101} faces, the materials synthesized are likely to behave differently under irradiation and, consequently, have different photocatalytic

activity. Specifically, since the {001} facets in TiO₂ are known to be more oxidizing, we expected the COOH-GNP-TiO₂ composite material to be more efficient at phenol abatement than the NH₂-GNP-TiO₂ material.

We tested phenol abatement on all materials reported in Table 1. Preliminary experiments on pristine GNP, COOH-GNP and NH₂-GNP allowed us to determine the best experimental conditions: due to their dark color, we resorted to use only a very low concentration of these materials (25-50 mg L⁻¹), whereas we could increase the catalyst concentration up to 1g L⁻¹ for the hybrid materials containing also TiO₂.

Adsorption experiments in the dark showed that phenol was poorly adsorbed on all materials (Figure S2). Direct photolysis scarcely contributed to the phenol transformation, too: its degradation was negligible even after long irradiation times, as previously reported³⁴.

Phenol disappearance curves are plotted in Figure 1A. GNP and functionalized GNP (COOH-GNP and NH₂-GNP) were not able to induce the photo-degradation of phenol, causing only less than 10% phenol degradation during 2 hours of irradiation. Pure TiO₂ (TiO₂) was able to completely abate phenol within 2 hours.

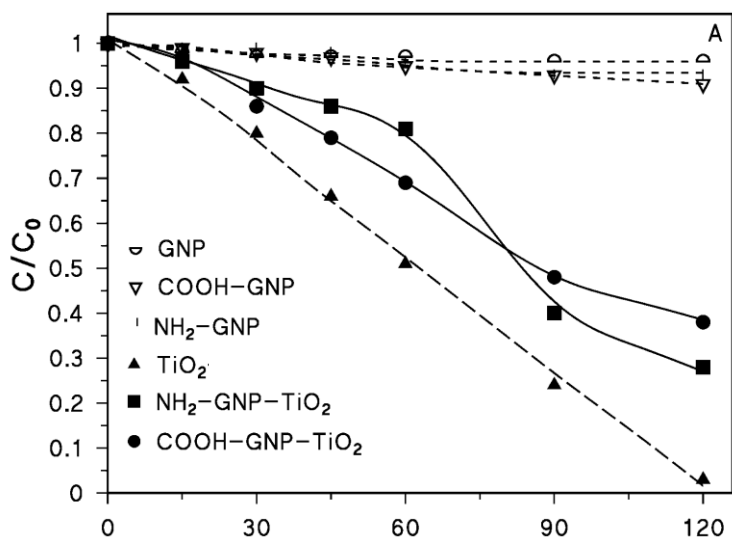
In the presence of COOH-GNP-TiO₂ and NH₂-GNP-TiO₂, the degradation was initially very slow (only 15% of phenol was abated during the first 30 min), then sped up (after 90 min, 50% or 60% of phenol disappears in the presence of COOH-GNP-TiO₂ or NH₂-GNP-TiO₂, respectively), and then, again, slowed down (after 2 h of irradiation, 40% and 30% of phenol was still present, in the presence of COOH-GNP-TiO₂ or NH₂-GNP-TiO₂, respectively). This behavior could be attributed to a modification of the materials or of the photogenerated reactant species occurring during irradiation. In fact, both COOH-GNP-TiO₂ and NH₂-GNP-TiO₂ changed color within a few minutes since the beginning of irradiation, and the grey suspensions turned to pale grey (Figure S3); however, after 30 min of irradiation the materials seemed to stabilize, and did not further change color.

To understand the importance of this material transformation upon irradiation, we irradiated both COOH-GNP-TiO₂ and NH₂-GNP-TiO₂ for 30 min or 1 h without phenol and then repeated the experiments with phenol. The results are plotted in Figure 1B, where COOH-GNP-TiO₂ UV-A activated materials are compared with pristine TiO₂. The two curves obtained after 30 min or 1 h of pre-irradiation following addition of phenol at 10 mg/L are very similar, thus confirming the stabilization of the material suggested above. Phenol was degraded faster on the activated COOH-GNP-TiO₂ than on TiO₂ at the beginning of the experiment: almost 60% of phenol (C₀=10 mg/l) was degraded within 5 min of irradiation, and 80% phenol degradation was achieved within 30 min. A similar initial faster degradation followed by a slower reaction was found on the activated NH₂-

GNP-TiO₂ (see fig. S4), although the overall degradation on this sample was much lower than on COOH-GNP-TiO₂. Thus, while before activation we could not observe a strong difference in photocatalytic efficiency between NH₂-GNP-TiO₂ and COOH-GNP-TiO₂, after UV-A activation COOH-GNP-TiO₂ became much more efficient than NH₂-GNP-TiO₂. This agrees with what we were expecting, since more oxidizing TiO₂ facets are exposed toward the solution in the COOH-GNP-TiO₂ sample.

We hypothesize that the reason for the instability of NH₂-GNP-TiO₂ and COOH-GNP-TiO₂ under irradiation and the different phenol degradation rates observed for these materials (Figure 1A) is that some of the photogenerated species reacted with the hybrid materials. Photodegradation of reduced graphene oxide was indeed previously observed by Kamat and coworkers, especially for prolonged irradiation experiments, whereas for brief irradiations and in the presence of probes which can be easily oxidized and abated, such as Methylene Blue or Rhodamine B, photocatalytic degradation of graphene is seldom observed.³⁵ In our case the long irradiation experiments, necessary for phenol abatement, led to a change in the materials (Figure S3), and a decrease in their photocatalytic activity. By pre-irradiating the samples (Figure 1B), we completed the material transformation before phenol addition, thus allowing the phenol to be degraded in the absence of any competitive reaction.

The activated COOH-GNP-TiO₂ sample was much more effective at degrading phenol than the control TiO₂-TEOA sample at early degradation times (Figure 1B). However, the kinetics slowed down at longer irradiation time, showing a trend that is consistent with a second-order kinetics where a reactant is limiting. To understand this phenomenon, we measured phenol degradation on these samples at different initial phenol concentrations (20 mg L⁻¹, plotted in Figure 1B).



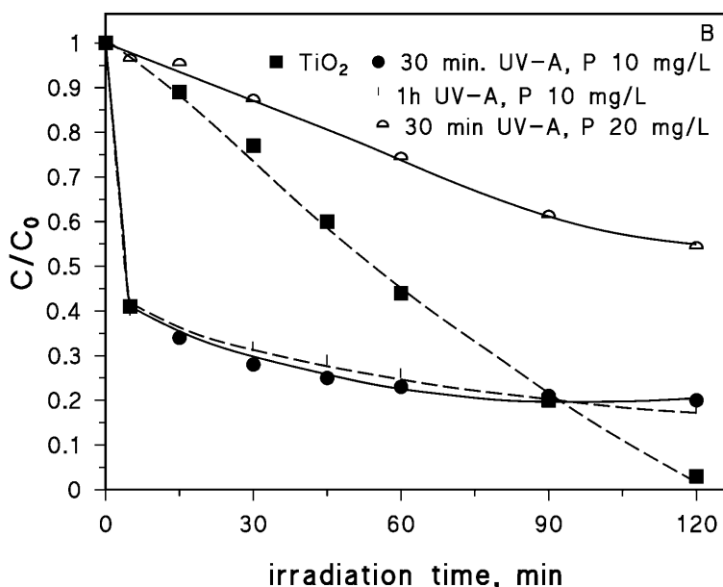


Figure 1. Phenol (P) disappearance as a function of irradiation time. The conditions in all experiments are the following: (A) P 10 mgL⁻¹; GNP (25 mg L⁻¹), COOH-GNP (25 mg L⁻¹), NH₂-GNP (25 mg L⁻¹), TiO₂ (1 g L⁻¹), NH₂-GNP-TiO₂ (1 g L⁻¹), COOH-GNP-TiO₂ (1 g L⁻¹); (B) pristine TiO₂ (1 g L⁻¹) and. P added after 30 min or 1h of COOH-GNP-TiO₂ (1 g L⁻¹) UV-A pre-irradiation (without P).

When the phenol concentration increased, the percentage of its abatement decreased and went from 80% to 46% on COOH-GNP-TiO₂. The concentration of phenol (P) as a function of irradiation time for a second order kinetics is expressed as:

$$\frac{P_t}{P_0} = \frac{P_0 - B_0}{P_0 - B_0 (e^{-k(P_0 - B_0)t})} \quad (1)$$

where P₀ is the initial phenol concentration and B₀ is the concentration of the limiting reactant. By introducing R=(A₀-B₀)/A₀, equation (1) can be expressed as:

$$\frac{P_t}{P_0} = \frac{R}{1 - (1-R)e^{-kRP_0t}} \quad (2)$$

From the data plotted in Figure 1B, B₀ can be calculated as 8.6±0.5 mg L⁻¹. Considering that oxygen content in GNP-COOH is very low (2.2%) and that a GNP content below 5%, corresponding to a concentration lower than 50 mg L⁻¹, is estimated in the hybrid samples³¹, the limiting defective (and very reactive) species reactant can be ascribed to GNP itself rather than the functional groups on GNP.

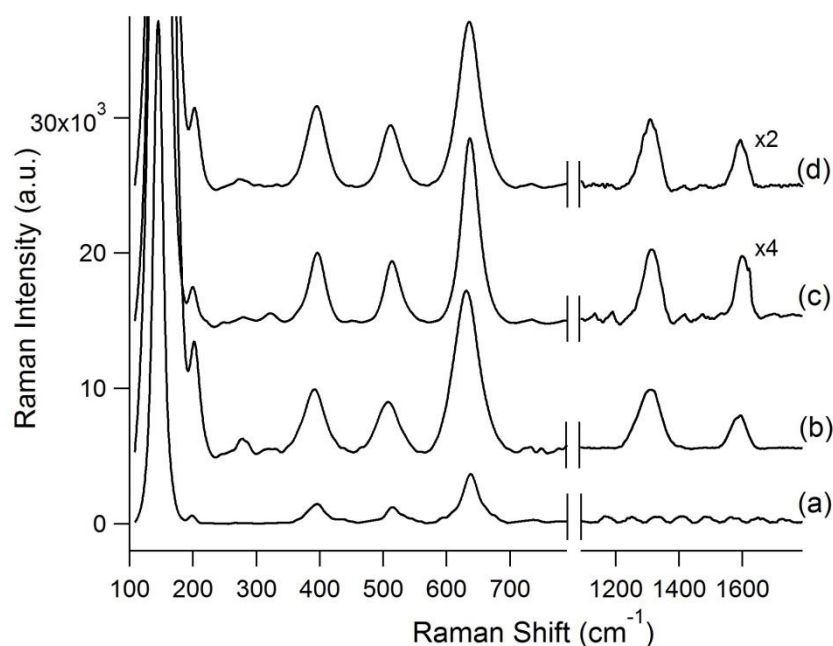
3.2 Photo-induced phenol degradation with functionalized GNP/TiO₂ hybrids synthesized in the presence of shape controllers

To better control the morphology of the TiO₂ NPs in the GNP-TiO₂ hybrids and attempt to stabilize them, we introduced shape controllers in solution during the hydrothermal synthesis. We selected either ethylenediamine (EDA) or oleic acid (OA), because they are known to favor the growth of different crystalline facets ({100} and {101} for EDA and {001} for OA³²). These facets will be oriented towards the solution, thus affecting the charge carrier separation process and therefore the photoactivity and the stability of the hybrid materials.³¹

3.2.1. Material characterization

Figures 2 and S5 show the Raman spectra of COOH-GNP-TiO₂ and NH₂-GNP-TiO₂ prepared with EDA (COOH-GNP-TiO₂-EDA) or OA (COOH-GNP-TiO₂-OA) as shape controllers. The spectra are quite similar to those observed for the samples prepared in the absence of shape controllers³¹, and show that only anatase phase was formed during the hydrothermal synthesis. Five well resolved peaks can be identified in the range 150-650 cm⁻¹, localized at 144 cm⁻¹ (E_g), 197 cm⁻¹ (E_g), 395 cm⁻¹ (B_{1g}), 513 cm⁻¹ (B_{1g}+A_{1g}) and 634 cm⁻¹ (E_g)³⁶, consistent with the characteristic vibrations for anatase. Additionally, two peaks at 1594 cm⁻¹ and 1320 cm⁻¹ are observed, which can be attributed to the GNP substrate: the peak at 1594 cm⁻¹ corresponds to the Raman-active mode with symmetry E_{2g} and it is characteristic of the presence of sp² C in graphene (G band), while the peak at 1320 cm⁻¹ is associated with the presence of defects in the hexagonal C lattice (D band). The intensity ratio between TiO₂-related bands and G and D bands gives a qualitative measurement of the degree of association between TiO₂ and GNP, which decreases in the order NH₂-GNP-TiO₂-OA > COOH-GNP-TiO₂-OA > COOH-GNP-TiO₂-EDA >> NH₂-GNP-TiO₂-EDA, for which close association between TiO₂ and GNP can be excluded.

Figure 2. Raman spectra of NH₂-GNP-TiO₂-EDA (a), NH₂-GNP-TiO₂-OA (b), COOH-GNP-TiO₂-EDA (c), and COOH-GNP-TiO₂-OA (d).



Figures 3-6 show the TEM images of all the samples prepared in the presence of shape controllers. The sample COOH-GNP-TiO₂-EDA shows both small (40-60 nm) and large (>100 nm) particles (Figure 3). The smaller particles appear as rounded squares. These are likely to be truncated bipyramids with their *c* axis pointing outside the plane of the image³⁷, which makes it hard to understand the extension of their crystalline facets. The bigger particles are quite elongated; since Raman shows that these are anatase, we can deduce that the {100} facets are more developed on these particles than the {101} facets. None of the TEM images showed TiO₂ NPs associated with GNP, thus suggesting that EDA favors homogeneous rather than heterogeneous nucleation.

On COOH-GNP-TiO₂-OA, most images show that the TiO₂ NPs are supported on GNP, which implies that the NPs nucleated and grew directly on graphene (Figure 4). The particles are less elongated than those observed on COOH-GNP-TiO₂ (Figure S1A and ³¹, i.e. with a larger truncation ratio, and their projection on the micrograph is often a square. This implies that the presence of OA favors the growth of {100} and {001} facets at the expenses of the {101}³², giving the particles a pseudo-cubic appearance. The layer spacing is 0.36 nm (Figure 4D; this is the characteristic spacing for anatase (101) planes, which can be detected on both {101} and {001} facets. This implies that the crystalline facet shown in Figure 4d can be either the {101} facet of a bipyramid lying on the opposite {101} facet, or the top {001} facet of a particle with its *c* axis directed towards the observer (see Scheme 1).

Similar considerations hold for the amino functionalized samples: when EDA is added as shape controller (NH₂-GNP-TiO₂-EDA), elongated particles are obtained (Figure 5). The spacing detected in Fig 5b is again characteristic of the anatase (101) planes, and can be present on both {101} and

{001} facets as discussed above. No evidence of GNP binding was observed, so that we can conclude that a homogeneous nucleation occurred.

Similarly to what observed on COOH-GNP-TiO₂-OA, the TiO₂ NPs nucleate and grow directly on GNP on the NH₂-GNP-TiO₂-OA sample. However, the NPs are less square, and their truncated bipyramidal shape is more evident. High resolution images show again a plane spacing of 0.34 nm. However, since in this case the facets are trapezoidal, this spacing must be referred to (101) planes found on {101} facets, thus suggesting a larger development of these facets on this sample.

A summary of the effect of the shape controllers on particle morphology is shown in Scheme 3. One of the main differences between the samples formed in the presence of OA and EDA is that those synthesized with EDA do not show TiO₂ NPs associated with GNP. This is consistent with the Raman results evidencing little (Figure 2c) or no (Figure 2a) presence of graphene peaks associated to TiO₂ NPs in the case of COOH-GNP-TiO₂-EDA and NH₂-GNP-TiO₂-EDA, respectively. We can explain this considering that EDA can easily be adsorbed on TiO₂ surface by forming EDA/TiO₂ complexes³⁸. To prove this, we added EDA dropwise to a TiO₂ suspension; the well-dispersed suspension turned to deeply aggregated particles that settled down, as displayed in Figure S6, thus leading to more hydrophobic TiO₂ NPs. We hypothesize that this phenomenon isolates GNP from TiO₂ NPs, and that this in turn may prevent GNP degradation upon irradiation, while still maintaining the advantages of fast phenol degradation kinetics shown by the previous composites.

To prove this point, we proceeded with the phenol degradation tests in the presence of COOH-GNP-TiO₂-EDA, NH₂-GNP-TiO₂-EDA, COOH-GNP-TiO₂-OA, and NH₂-GNP-TiO₂-OA.

Figure 3: TEM micrographs of COOH-GNP-TiO₂-EDA, scale bar is 100 nm in all panels

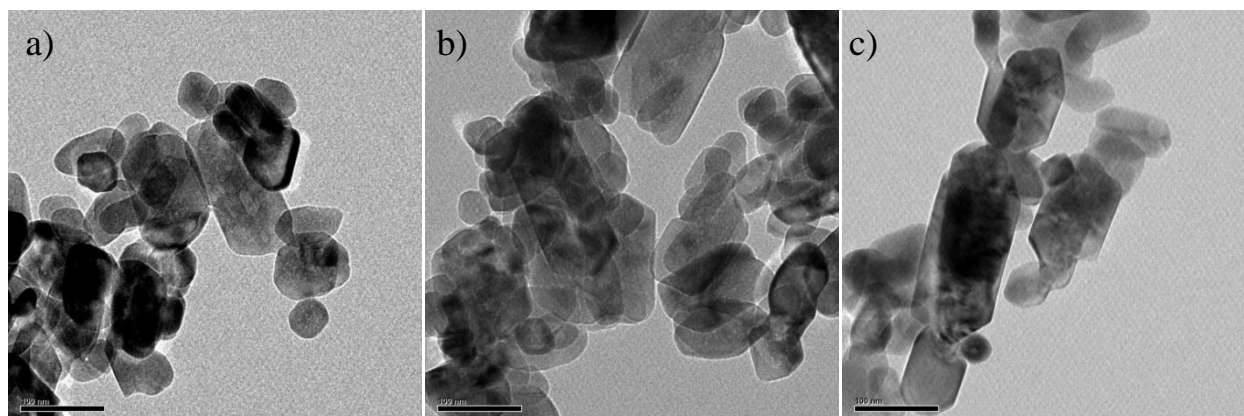


Figure 4: Low (a) and high (b,c,d) magnification TEM micrographs of COOH-GNP-TiO₂-OA.

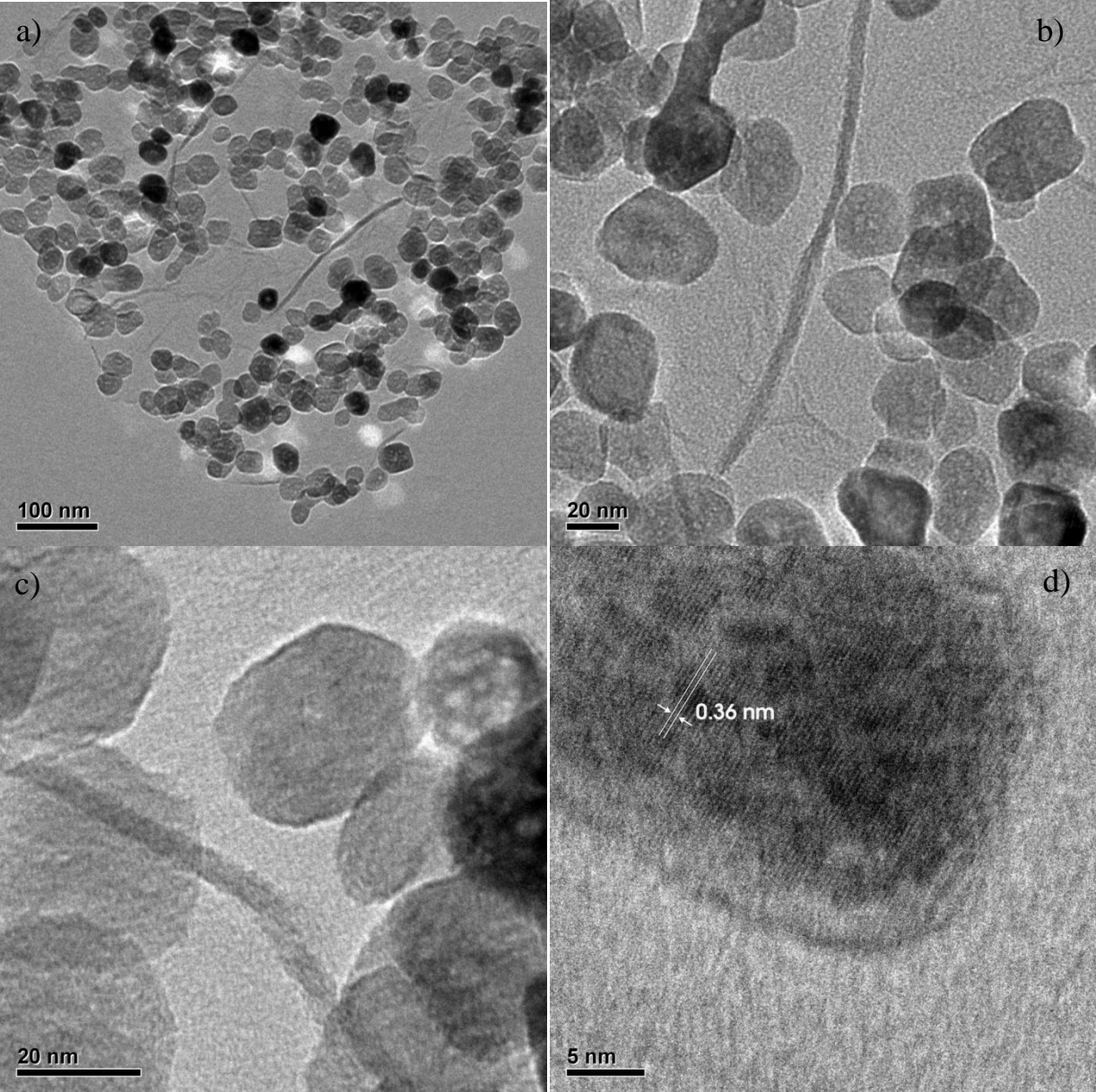


Figure 5: Low (a) and high (b) magnification TEM micrographs of $\text{NH}_2\text{-GNP-TiO}_2\text{-EDA}$

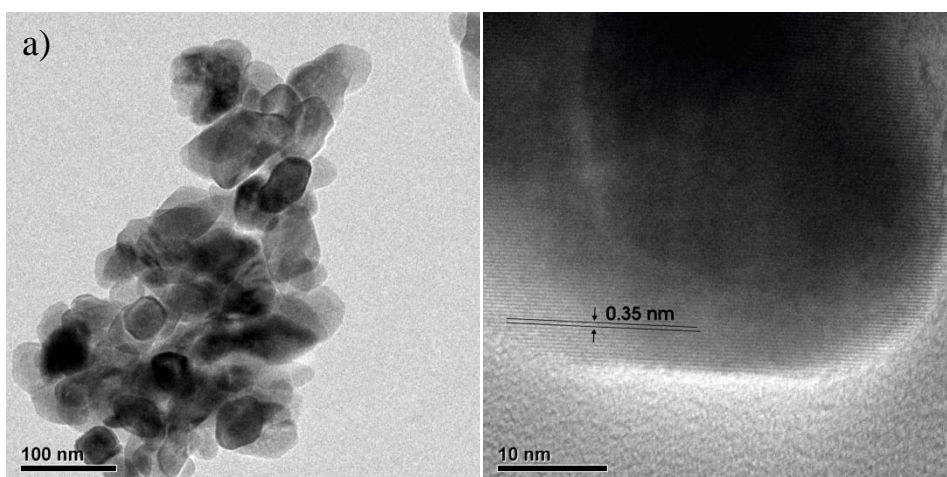
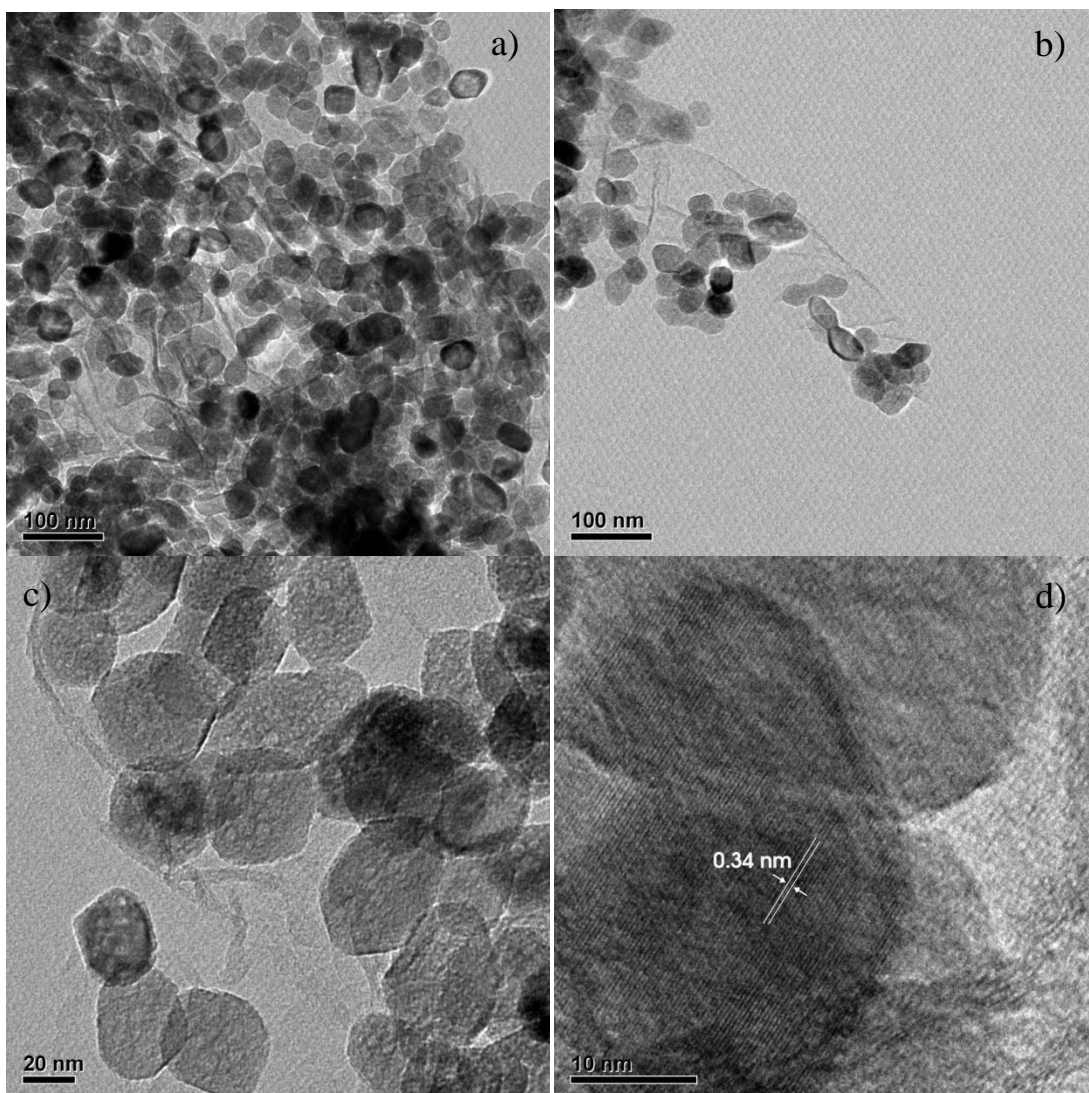
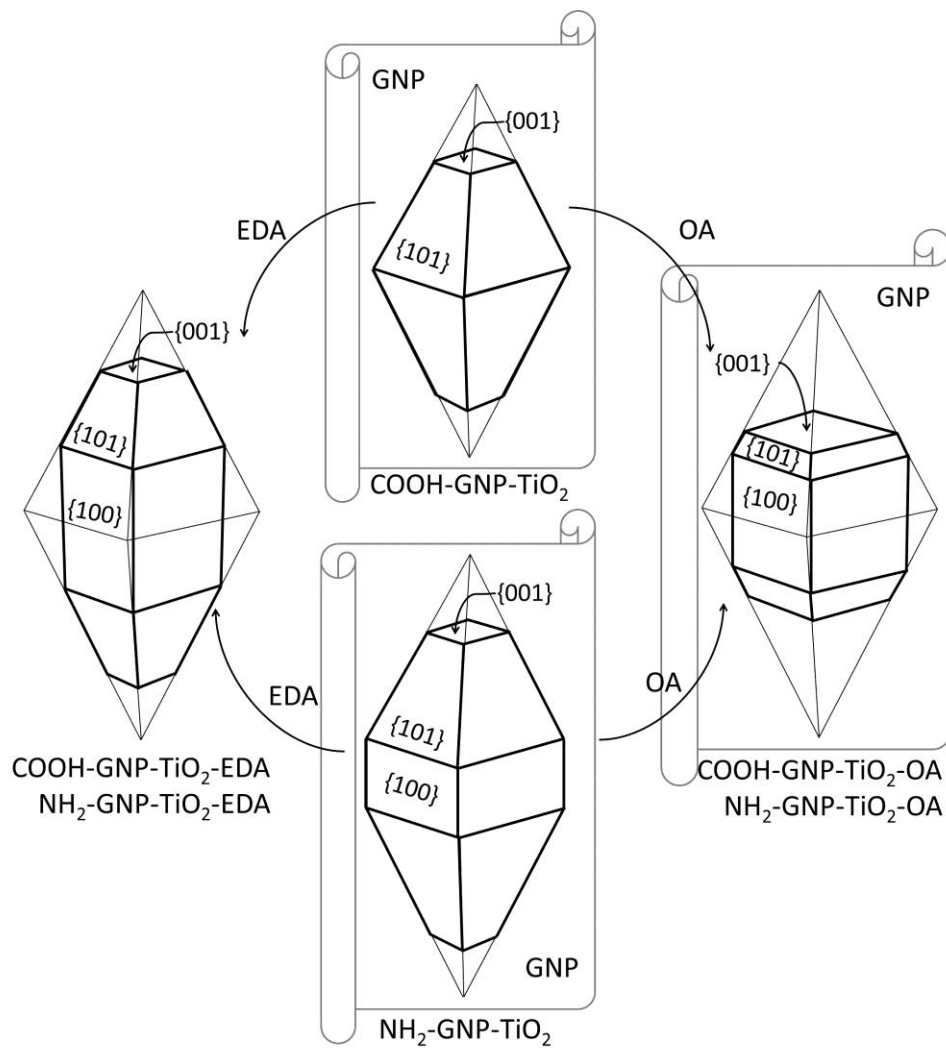


Figure 6: Low (a,b) and high (c,d) magnification TEM micrographs of $\text{NH}_2\text{-GNP-TiO}_2\text{-OA}$





Scheme 3: Representation of the dominant particle morphology found in GNP-TiO₂ hybrid materials. While EDA leads to elongated, rod-like particles, OA favors pseudo cubic shape. In the presence of EDA, homogeneous nucleation is favored over heterogeneous nucleation on GNP, which is instead observed in the presence of OA.

3.2.2 Photocatalytic tests

The results of the photocatalytic degradation of phenol on the hybrid materials prepared with EDA and OA are shown in Figure 7. Differently from $\text{NH}_2\text{-GNP-TiO}_2$ and COOH-GNP-TiO_2 , all materials were stable under irradiation; no changes in color and in UV-Vis spectra were observed, even after long irradiation times.

The addition of shape controllers to COOH-GNP-TiO_2 (Figure 7A) led to different results: while EDA improved the photocatalytic efficiency, OA had a detrimental effect. Within 120 min of irradiation, only 40% of phenol was abated on $\text{COOH-GNP-TiO}_2\text{-OA}$. Complete phenol degradation was achieved within 90 min of irradiation on $\text{COOH-GNP-TiO}_2\text{-EDA}$, while this took 120 min on TiO_2 . The low activity observed for $\text{COOH-GNP-TiO}_2\text{-OA}$ may be attributed to the adsorption of OA on TiO_2 surfaces, leading to its inactivation. In fact, aliphatic carboxylic acids are known to adsorb on TiO_2 anatase and are employed in dye sensitized solar cells to avoid direct contact between TiO_2 and electrolyte thereby enhancing cell stability³⁹.

The addition of shape controllers to $\text{NH}_2\text{-GNP-TiO}_2$ (Figure 7B), instead, did not improve the photocatalytic efficiency of this sample; in particular, $\text{NH}_2\text{-GNP-TiO}_2\text{-OA}$ showed the lowest activity. Since the sample $\text{NH}_2\text{-GNP-TiO}_2\text{-OA}$ shows morphology similar to $\text{NH}_2\text{-GNP-TiO}_2$ without the addition of shape controller, we do not expect, on the basis of the morphological analysis, an improvement in efficiency and stability under irradiation.

The fast kinetics observed in the presence of $\text{COOH-GNP-TiO}_2\text{-EDA}$ (pseudo-first order kinetics similar to what observed on TiO_2 , with $t_{1/2}$ of 30 min for the hybrid catalyst and $t_{1/2}$ 55 min for TiO_2) must be related to the preferential growth of more oxidizing {100} facets obtained in the presence of EDA, the more effective and selective hole transfer to phenol induced by the synthesis in the presence of COOH-GNP , and the material stabilization due to the separation of GNP from TiO_2 NPs (Figure 3) due to the presence of EDA. However, this result questions the role of GNP in improving the photocatalytic activity of TiO_2 : if GNPs are separated from TiO_2 , do they participate at all in the photocatalytic experiment?

To answer this question, we synthesized TiO_2 in the presence of EDA but without GNP (sample $\text{TiO}_2\text{-EDA}$), and tested this material for its photocatalytic activity. The results for this material are plotted in Figure 7A for comparison. We see a rate of phenol abatement very similar for TiO_2 and $\text{TiO}_2\text{-EDA}$, in both cases much lower than in the presence of $\text{COOH-GNP-TiO}_2\text{-EDA}$ particles. This proves that GNP plays a crucial role in increasing phenol degradation rate when $\text{COOH-GNP-TiO}_2\text{-EDA}$ particles are used, while EDA is responsible mostly for providing a loose coupling with GNP thus reducing its degradation.

The strong differences observed between COOH-GNP-TiO₂-EDA and COOH-GNP-TiO₂-OA seem to indicate that while OA non-specifically adsorbs on all TiO₂ facets, EDA complexes specifically the less active {101} facets, while the most active (and oxidative) {001} facets remain free.³²

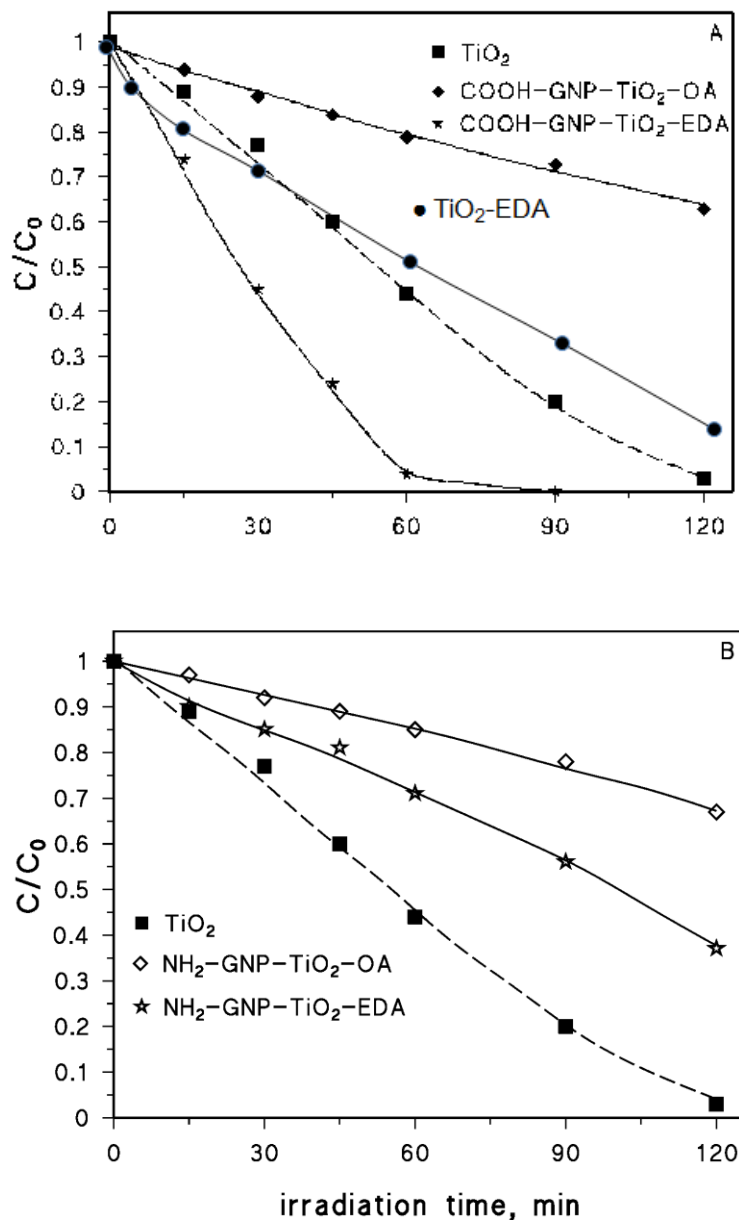


Figure 7. Phenol ($C_0 = 10 \text{ mgL}^{-1}$) disappearance as a function of irradiation time on materials prepared with shape controllers. (A) TiO₂ (1 gL^{-1}), TiO₂-EDA (1 gL^{-1}), TiO₂-OA (1 gL^{-1}), COOH-GNP-TiO₂-OA (1 gL^{-1}), COOH-GNP-TiO₂-EDA (1 gL^{-1}); (B) TiO₂ (1 gL^{-1}), NH₂-GNP-TiO₂-EDA (1 gL^{-1}), NH₂-GNP-TiO₂-OA (1 gL^{-1}).

Conclusions

We have shown phase and shape control of TiO₂ NPs grown on carboxylic and amino functionalized GNP, in the presence of OA and EDA in solution as further shape controllers and material stabilizers. Among all materials synthesized, the COOH-GNP-TiO₂ hybrid prepared by adding EDA as shape controller exhibits the best performance toward phenol abatement, with almost twice as fast kinetics of phenol degradation than TiO₂ alone. We ascribed this result to the better charge carrier separation and loose coupling between COOH-GNP and TiO₂ NPs stabilized by EDA. The proximity between COOH-GNP and the reducing {101} facets of TiO₂ led to a more efficient transfer of photoelectrons, which in turn reduced charge recombination and improved the photoreduction reaction yield, while the lack of contact between the GNPs and the TiO₂ prevented GNP degradation during the process. This result paves the road for a new generation of hybrid photocatalysts, which achieve better results thanks to their carefully controlled architecture.

Acknowledgments

This research is supported by a Marie Curie International Research Staff Exchange Scheme Fellowship (PHOTOMAT, proposal n. 318899) within the 7th European Community Framework Programme, the Natural Sciences and Engineering Research Council of Canada (NSERC), Fonds de recherche du Québec – Nature et technologies (FRQNT), Center for Self-assembled Chemical Structures (CSACS), Canada Research Chairs (CRC), the Canada Foundation for Innovation (CFI), and McGill Engineering Doctoral Award (MEDA).

References:

1. A. Fujishima, K. Hashimoto, T. Watanabe, (1999) "TiO₂ Photocatalysis, Fundamentals and Applications", Bkc Inc., Tokyo
2. I.K. Konstantinou and T.A. Albanis, *Appl. Catal. B Environ.*, 2003, **42**, 319-335
3. T. L. Thompson and J. T. Yates, *J. Chem. Rev.*, 2006, **106**, 4428–4453
4. P. Calza, V.A. Sakkas, C. Medana, A. Azharul Islam, E. Raso, K. Panagiotou and T. Albanis, *Appl. Catal. B Environ.*, 2010, **99**, 314-320

5. C. Minero, G. Mariella, V. Maurino and E. Pelizzetti E., *Langmuir*, 2000, **16**, 2632-2641
6. N. Serpone and E. Pelizzetti, *Photocatalysis fundamentals and applications*, 1989, Wiley Interscience, Amsterdam
7. X. Chen and S.S. Mao, *Chem. Rev.*, 2007, **107**, 2891-959
8. Y. Liu, L. Chen, J. Hu., J. Li and R. Richards, *J. Phys. Chem. C*, 2010, **114**, 1641-1645
9. S. Livraghi, M.C. Paganini, E. Giamello, A. Selloni, C.D. Valentin and G. Pacchioni, *J. Am. Chem. Soc.*, 2006, **128**, 15666-15671
10. H. Wang, T. You, W. Shi, J. Li and L. Guo, *J. Phys. Chem. C*, 2012, **116**, 6490-6494
11. S. Hoang, S.P. Berglund, N.T. Hahan, A.J. Bard and C.B. Mullins, *J. Am. Chem. Soc.*, 2012, **134**, 3659-3662
12. H. Kim, J. Kim and W. Choi, *J. Phys. Chem. C*, 2011, **115**, 9797-9805
13. G.M. Veith, A.R. Lupini and N.J. Dudney, *J. Phys. Chem. C*, 2009, **113**, 269-280
14. J.C. Yu, G. Li, X. Wang, X. Hu, C.W. Leung and Z. Zhang, *Chem. Commun.* 2006, **25**, 2717-2719.
15. J.R. Raji and K. Palamivelu, *Ind. Eng. Chem. Res.* 2011, **50**, 3130-3138
16. W. Han, P. Liu, R. Yuan, J. Wang, Z. Li, J. Zhuang and X. Fu, *J. Mat. Chem.*, 2009 **19**, 6888-6895
17. Y.J. Xu, Y. Zhuang and X. Fu, *J. Phys. Chem. C*, 2010, **114**, 2669-2676
18. F. Zhang, X. Carrier, J.M. Krafft, Y. Yoshimura and J. Blanchard, *New J. Chem.*, 2010, **34**, 508
19. Q. Xiang, J. Yu and M. Jaroniec, *J. Am. Chem. Soc.*, 2012, **134**, 6575-6578
20. H. Zhang, X. Lu, Y. Li and J. Wang, *ACS Nano*, 2011, **5**, 590-596
21. K. Li, J. Xiong, T. Chen, L. Yan, Y. Dai, D. Song, Y. Lu and Z. Zeng, *J. Hazar. Mat.*, 2013, **250**, 19-28
22. K. Li, T. Chen, L. Yan, Y. Dai, Z. Huang, J. Xiong, D. Song, Y. Lu and Z. Zeng, *Colloid. Surf. Physic. Engineer. Aspc.*, 2013, **422**, 90
23. O. Akhavan and E. Ghaderi, *J. Phys. Chem. C*, 2009, **113**, 20214-20220
24. H. Wang, T. Maiyalagan and X. Wang, *ACS Catal.*, 2012, **2**, 781-794
25. U. Diebold, *Surf. Sci. Rep.*, 2003, **48**, 53-229.
26. T. Taguchi, Y. Saito, K. Sarukawa, T. Ohno and M. Matsumura, *New J. Chem.*, 2003, **27**, 1304-1306.
27. C. Z. Wen, H. B. Jiang, S. Z. Qiao, H. G. Yang and G. Q. Lu, *J. Mater. Chem.*, 2011, **21**, 7052-7061.
28. T. Tachikawa, N. Wang, S. Yamashita, S.-C. Cui and T. Majima, *Angewandte Chemie International Edition*, 2010, **49**, 8593-8597.

29. T. Ohno, K. Sarukawa and M. Matsumura, *New J. Chem.* 2002, **26 (9)**, 1167-1170
30. P.V. Kamat, *J. Phys. Chem. Lett.* 2011, **2(3)**, 242-251
31. F. Sordello, G. Zeb, K. Hu, P. Calza, C. Minero, T. Szkopek and M. Cerruti, *Nanoscale*, 2014, **6**, 6710-6719
32. T. Sugimoto, X. Zhou and A. Muramatsu, *J. Colloid Interface Sci.* 2003, **259 (1)**, 53-61
33. K.J. Huang, D.J. Niu., X. Liu, Z.W. Wu, Y.F Fan and Y.Y.Wu, *Electrochimica Acta*, 2010, **56**, 2947-2953
34. P. Calza, L. Rigo and M. Sangermano, *Appl Cat B: Environ.*, 2011, **106**, 657-665.
35. J. G. Radich, A. L.Krenselewski, J. Zhu, P. V. Kamat, *Chem. Mater.* 2014, **26 (15)**, 4662-4668
36. T. Ohsaka, F. Izumi and Y. Fujiki, *J. Raman Spectrosc.* 1978, **7**, 321-324
37. C. Deiana,; M. Minella, G. Tabacchi, V. Maurino, E. Fois and G. Martra, *Phys. Chem. Chem. Phys.* 2013, **15 (1)**, 307-315
38. E. Farfan-Arribas and Robert J. Madix, *J. Phys. Chem. B*, 2003, **107**, 3225-3233
39. J. Lim, Y.S. Kwon, T. Park, *Chem. Commun.*, 2011, **47**, 4147-4149